

PIV measurement in a four-roll-mill flow with a central difference image correction (CDIC) method

S. T. Wereley, L. Gui

Abstract An experiment is conducted in a four-roll mill to verify a novel PIV recording evaluation algorithm that combines the central difference interrogation and image correction techniques. Simulations and experiments in the four-roll mill geometry demonstrate that the central difference image correction method described in this paper can not only minimize the bias error resulting from the curvature and high velocity gradient flow but can also effectively reduce the random error resulting from the particle image pattern distortion. In addition, the new algorithm can substantially reduce the peak-locking effect in digital PIV image evaluation by using a continuous window shifting technique. The PIV experiment accurately determines the velocity field in the four-roll mill and confirms the linear distributions of the velocity components in the four roll mill as well as their dependence on the roller speed.

1

Introduction

The four-roll mill is a device proposed by G.I. Taylor (1934) to study the breakup of small droplets in a viscous straining velocity field. It can produce a purely two-dimensional extensional flow and has proven to be a popular instrument for the study of drop deformation (Rumscheidt et al 1961; Higdon 1993), birefringence in polymer solutions (Guller and Leal 1981), and flow-induced crystallization in polymer melts (Torza 1975). Bentley and Leal (1986) designed a computer controlled four-roll mill capable of producing arbitrary linear flow fields, holding droplets stationary in the center of the flow cell, and causing two droplets to interact. In the present work the PIV technique is used to investigate the flow in such a computer controlled four-roll mill. The four-roll mill generates a highly curved flow field, which causes significant image pattern distortion in the PIV recordings. In order to investigate the flow structure near the center of the device, i.e. the very low velocity region, large time intervals are usually used, so that relatively large particle image displacements are produced in the PIV recording pairs outside of the flow center. Therefore, window shifting and image pattern correction are necessary for evaluating PIV recordings obtained in the four-roll mill PIV experiment.

Currently, adaptive, discrete window shifting is widely used with the FFT-based correlation algorithm for reducing the evaluation error and with the image pattern tracking algorithms for increasing the spatial resolution. The adaptive window offset method, as typically implemented, can be referred to as a forward difference interrogation (FDI), because the second interrogation window is shifted in the forward direction of the flow an amount equal to the mean displacement of the particle images initially in the first window. Details of the FDI technique are described by Keane and Adrian (1993), Willert (1996), Cowen and Monismith (1997), and Westerweel et al. (1997). Although the adaptive window shifting method leads to significant improvements in the evaluation quality of PIV recordings in many cases, there are still some potentially detrimental bias errors that cannot be avoided with this technique. For instance, in a flow with large spatial gradients, attributing a measurement to the centroid of the first interrogation region (FDI assumption) can lead to significant errors when compared to its proper location—at the centroid of both interrogation regions. A central difference interrogation (CDI) method was introduced by Wereley, et al., (1998) and further developed and explored by Wereley and Meinhart (2000, 2001), to avoid the shortcomings of FDI and increase the accuracy of the PIV measurement. When using CDI, the first and the second interrogation windows are shifted backward and forward, respectively, each by half of the expected particle image displacement. As multi-pass adaptive spatial shifting techniques, both FDI and CDI require some iteration to achieve optimum results. When properly programmed, using CDI does not cost more computation time than FDI. A recent study by Gui, et al (2001) indicates that the bias and random errors of the digital PIV recording evaluation can further be reduced by continuously, rather than discretely, shifting the interrogation windows according to preceding iterations. The peak-locking effect is also minimized with this technique. To account for the distortion of PIV image patterns in complex flow measurements, image correction techniques have been developed. The idea of image correction was first presented by Huang et al. (1993). Similar ideas were also applied by others. However, since the image correction was typically a complex and time-consuming procedure, it has not been widely used. In order to accelerate the evaluation, the authors combine a modified image correction method with the FFT-based correlation algorithm, so

that the evaluation error resulting from the image pattern distortion can be effectively reduced with only minimal additional computation time, i.e. a fraction of the regular evaluation time. Named the central difference image correction (CDIC) method in this paper, the new evaluation algorithm combines ideals of central difference interrogation, adaptive continuous window shifting and image correction, and enables a most reliable and accurate evaluation of digital PIV recordings. Details are provided below.

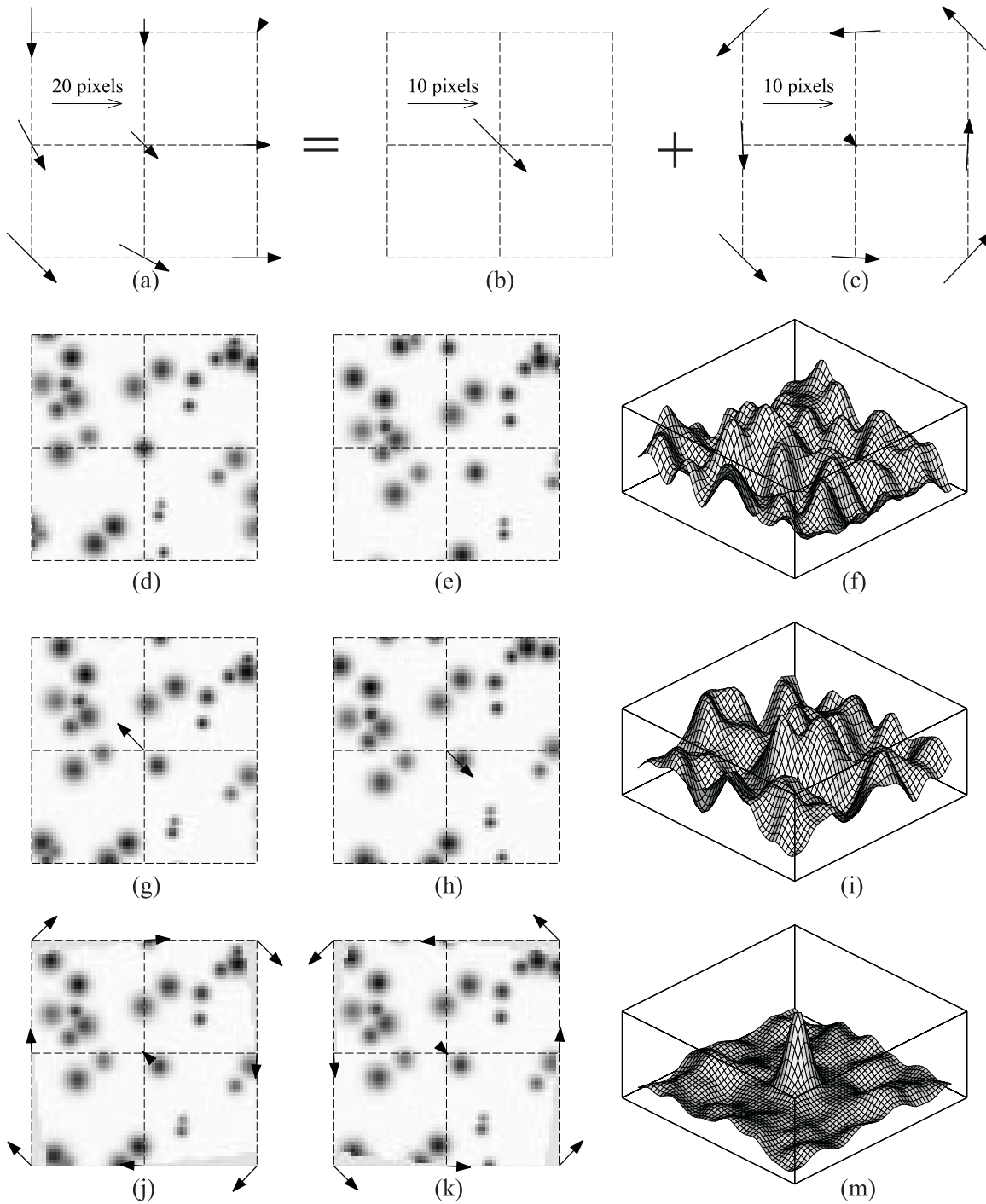


Fig. 1: Interrogation window shift and image pattern correction

2

Central Difference image correction

The idea of central difference image correction is demonstrated in Fig. 1 by evaluating a synthetic PIV image pair near a strong vortex center with a 64×64 -pixel interrogation window and a 50% overlap. The velocity distribution on a small 3 by 3 interrogation grid (Fig. 1a) can be decomposed into a translational movement (Fig. 1b) and distortion (Fig. 1c). When using a traditional cross-correlation algorithm with no window shifting, the evaluation sample pair is obtained with both interrogation windows centered at the evaluation point, e.g. Fig. 1d and 1e for the central point of 3×3 grid. The traditional correlation method works well in cases of small particle image displacement and relatively simple flow. But in the current case the image patterns in the sample pair do not match well, so that the correlation function (Fig. 1f) does not show a dominant peak for the particle image displacement. Considering the translation movement of the particle images in the evaluation sample pair, the interrogation windows for the first and second recording can be shifted backwards and forwards, respectively, to realize a central difference interrogation, see Fig. 1g and 1h, so that the image patterns match better to each other. However, the correlation function still does not present a very clear peak to reliably and accurately determine the particle image displacement (Fig. 1i). When considering the particle image distortion, i.e. pre-deforming the image patterns forwards and backward respectively for the first and second evaluation sample (Fig. 1j and 1k) based on the known displacements at the 9 grid points, a very good match of the image patterns is realized, so that a correlation function with a clear main peak is obtained (Fig. 1m). Although in this demonstration the window shifting and the image pattern correction are carried out in two steps, they can be realized in only one step in practical applications.

When using the FFT algorithm to accelerate the calculation, the correlation-based evaluation function is usually written as

$$\Phi(m, n) = \sum_{i=1}^M \sum_{j=1}^N g_1(i, j) \cdot g_2(i+m, j+n) \quad (1)$$

where g_1 and g_2 are gray value distributions of the two evaluation samples, which are restricted in a rectangular interrogation window of size of $M \times N$ pixels. For traditional correlation algorithms with or without discrete window shifting, $g_1(i, j)$ and $g_2(i, j)$ are extracted directly from the discrete gray value distributions of the PIV recording pair $G_1(i, j)$ and $G_2(i, j)$, respectively. However, when using the central difference image correction, the shifts of pixels in the interrogation windows are not limited to discrete integer values and, in most cases, are not constant across the windows. We assume that the displacement of the image pattern at pixel (i, j) in the interrogation window is determined as $X(i, j)$ and $Y(i, j)$. The following bilinear interpolation function is used for determining the correlated function:

$$g(i, j) = (1-x) \cdot (1-y) \cdot G(i+I, j+J) + x \cdot (1-y) \cdot G(i+I+1, j+J) + y \cdot (1-x) \cdot G(i+I, j+J+1) + x \cdot y \cdot G(i+I+1, j+J+1) \quad (2)$$

wherein (I, J) and (x, y) are integer pixels and non-negative sub-pixel values, respectively; for $g=g_1$ and $G=G_1$: $I+x=-0.5X$, $J+y=-0.5Y$; for $g=g_2$ and $G=G_2$: $I+x=0.5X$, $J+y=0.5Y$. If $G(i, j)$ is limited in the $M \times N$ -pixel sampling window, there may not be enough information to completely fill the rectangular interrogation window, e.g. in Fig. 1j and 1k there are vacancy areas near the edges of the interrogation windows. However, since $G(i, j)$ is defined in the whole image plane, the interrogation window can be completely filled with PIV recording information in most cases. When the evaluation point is chosen at the edges of the PIV recording, padding or mask techniques (Gui and Merzkirch, 1996, 1998) can be used to deal with the vacancy area problem.

Because the particle image displacement (X, Y) is unknown before evaluation, initial values are taken to be zero or determined with previous knowledge of the flow. Then the evaluation is iterated until some convergence condition is fulfilled. Instead of determining the particle image displacement (X, Y) at every pixel in the interrogation window like the conventional image correction methods, displacements at the four corners (4-point method) or also at five center points (9-point method) of the interrogation window are used to determine the correction of the distorted image patterns. For the 4-point method the interrogation window is taken as one rectangular cell, whereas for the 9-point method there are four cells in the interrogation window. Within each rectangular cell, the displacement (X, Y) is determined with a bilinear interpolation function similar to Eq. (2). This simplification enables not only a fast image-corrected evaluation of the PIV recordings but also good convergence of the multi-pass evaluation algorithm. When using the 4-point image correction method, an adjustment is made, so that the displacement in the window center determines the translation movement and the displacements at the four corners determine the particle image pattern distortion.

The convergence of the CDIC method is tested here using a synthetically generated PIV recording pair with given particle image displacement $X=5\cos(j/256)$, $Y=5\cos(i/256)$ pixels. The synthetic particle images have a Gaussian gray value profile and are randomly distributed in PIV recordings of size of 1024×1024 pixels. The brightness of the particle image, i.e. the gray value in its center, is 130–250; the particle image diameter at the mid-

brightness cross section (FWHM) is 2–5 pixels; the particle image number is 20480, i.e. approximately 20 particles in a 32×32 -pixel interrogation window. This PIV recording pair is evaluated by using the above described 4- and 9-point image correction methods, respectively. Convergence factors and evaluation errors expressed as functions of iteration number are given in Fig. 2. The evaluation is conducted with a uniform grid and produces about 4000 displacement vectors. The convergence factor is here defined as a root-mean-square difference between the currently evaluated displacements and the displacements obtained in the previous iteration, whereas the RMS error is the root-mean-square difference between the evaluation results and the given particle image displacements. As shown in Fig. 2a, the evaluation procedures for both the 4-point and 9-point method converge after 6 iterations. Fig. 2b shows that the evaluation with the 4-point method converges at a much lower RMS error than that of the 9-point method. In an ideal case, evaluations are also conducted with given particle image displacements for the image correction without iterations, and the results show that the evaluation error of the 9-point method is somewhat smaller than that of the 4-point. However, the high accuracy of the 9-point method in the ideal case cannot be achieved in practical applications, where the particle image displacements are unknown.

In the above example the CDIC method is combined with the correlation-based interrogation algorithm, i.e. the same interrogation window size is applied to the two evaluation samples. Without any difficulty, the CDIC method can also be combined with the correlation-tracking algorithm, by which the second interrogation window is larger than the first one. As indicated in many previous studies, using the correlation-tracking algorithm is one way to avoid the large evaluation error of the correlation-based interrogation algorithm at large particle image displacements. However, The CDIC method applies a multi-pass continuous window shifting technique, so that the particle image displacement to be determined is near zero after a few iterations. Theoretically the evaluation error of the correlation-based interrogation algorithm is zero at zero displacement (Westerweel et al 1997), and it is usually much smaller than that of the correlation-tracking algorithm when the particle image displacement is within 0.5 pixels (Gui and Merzkirch 2000). In addition, with the same spatial resolution the correlation-tracking algorithm usually costs much more computation time than the correlation-based interrogation algorithm, because the former requires a larger computation window than the latter. Therefore, the combination of the central difference image correction and the correlation-based interrogation algorithm is a better choice. To defend this assertion, a test is conducted with a synthetic PIV recording pair that has the same particle images as in the previous example but smaller amplitude of the particle image displacement, i.e. 3 pixels. This synthetic recording pair is evaluated with combining the CDIC technique with the two correlation algorithms. The RMS evaluation errors at different iteration numbers are provided in Fig. 3. A 24×24 -pixel interrogation window is chosen for the correlation-based interrogation, and a padding method is used to enable the FFT acceleration (Gui and Merzkirch 1998). For the correlation tracking the first and second window are 24×24 and 32×32 pixels, respectively. Test results show that an obviously lower evaluation error is achieved when using the correlation-based interrogation scheme.

As indicated in Fig. 2 and 3, four or five iterations are necessary to achieve accurate evaluation results and further increasing the number of iterations will not provide significant improvements. In comparison to the FFT-based discrete window shifting techniques, the new algorithm needs 75% more computation time because of the

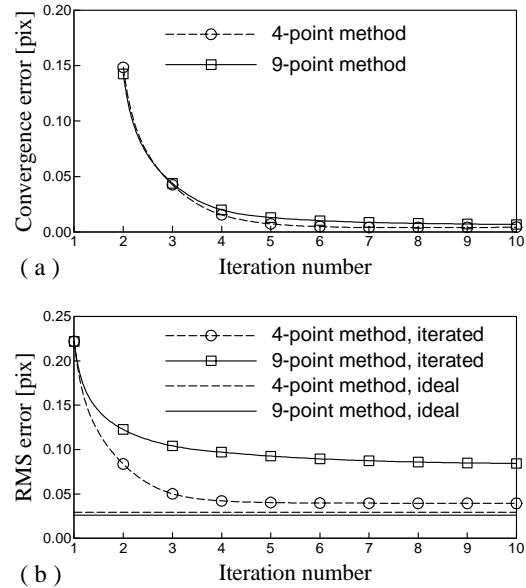


Fig. 2: Convergence of the image correction methods

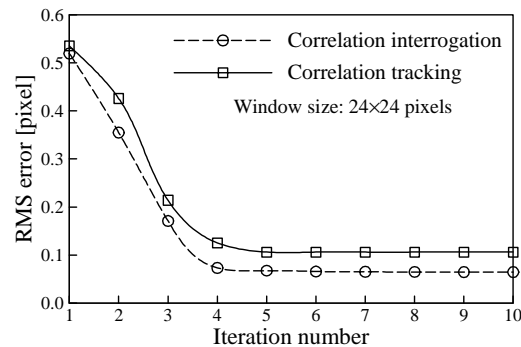


Fig.3: RMS errors of combining the image correction with two different correlation schemes

interpolations. However, because the CDIC is optimally combined with the correlation-based interrogation algorithm, large computation windows can be avoided, so that the computation time may be less than that of the adaptive discrete window shifting technique, as usually applied, in combination with the correlation tracking algorithm.

3 Four roll mill experiment

A top view of the four-roll mill device used for the test is shown in Fig. 4. It consists of four cylinder rollers of radius 7.2 mm, centered on the corners of a square of side 2×12.04 mm immersed in a square tank. The height of the rollers is 58 mm. The rotation of the cylindrical rollers is controlled in steps with a gear system, and the rotation angle for each step is 1.43×10^{-3} . The working fluid is Polyisobutylene. Extendspheres (SF14) produced by PQ Corporation, having a mean diameter of $55 \mu\text{m}$ and a density of 0.74g/cm^3 , are used as tracer particles. The measurement area of $9.48 \times 9.48 \text{ mm}^2$ centered within the four-roll mill is viewed by a Kodak ES1.0 camera with digital resolution of 1008×1008 pixels. The seeded flow is illuminated with a constant white light sheet. In the experiment the rotation of the cylinders is controlled at speed between 10–800 steps per second, so that the desired flow patterns are generated. Particle images are recorded in successive frames with given time interval between 50–4000 ms. The large time interval is suitable for the low roller speed and small time interval for the high speed, so that the maximal particle image displacement varies from 15 to 35 pixels.

To avoid large errors resulting from the low particle image number density, about nine image pairs are overlapped (Wereley et al., 2001) for each test case. As an example, the first image of the overlapped PIV recording pair for cylinder rotation speed of 10 steps/second and $\Delta t = 4$ s is shown in Fig. 5. Since in this case the velocity is very low, and the PIV images are consecutively recorded, the streamlines of the four-roll mill flow are visualized clearly. The overlapped PIV recording pair in this case is evaluated using the CDIC method with a 64×64 -pixel interrogation window, and the results are given in Fig. 6 in form of velocity vectors. Fig. 6 shows a symmetric flow pattern with low velocity in the center and high velocity at the corners, i.e. near to the rollers.

4 Accuracy of the new algorithm

4.1 Evaluation errors of FDI and CDI

The four-roll mill is used to generate a two-dimensional pure extensional flow with velocity field $u = Ax$, $v = -Ay$. For a given fluid A is a constant determined by the rotation speed of the rollers. In the first quadrant of the Cartesian coordinate system, the streamlines in the four-roll mill can be described as

$$x(t) = Ge^{At}, y(t) = Ge^{-At} \quad (3)$$

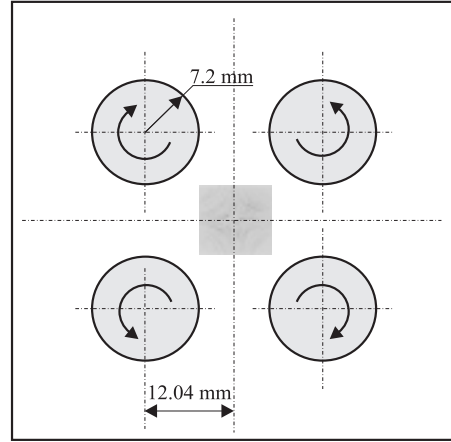


Fig. 4: Schematic diagram of the four-roll mill

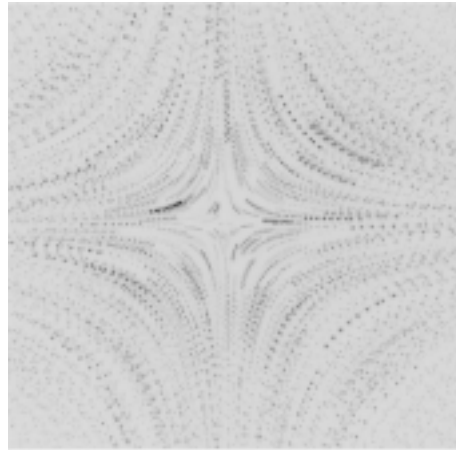


Fig.5: Overlapped PIV images (inverted) from the four-roll mill flow

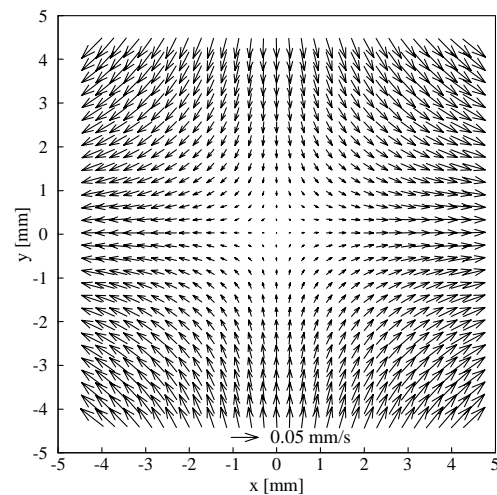


Fig.6: Vector map of the four-roll mill flow at cylinder rotation speed of 10 steps/second

with the origin ($t=0$) at ($x=G, y=G$), i.e. the intersection of the streamlines and line $x=y$. In the experiment the velocity component, for example u , can be approximately determined with the forward difference interrogation (FDI) and central difference interrogation (CDI), respectively, as

$$u_{FDI} = \frac{x(t + \Delta t) - x(t)}{\Delta t} \quad (4)$$

$$u_{CDI} = \frac{x(t + \Delta t / 2) - x(t - \Delta t / 2)}{\Delta t} \quad (5)$$

The bias errors of the two approximations are determined by using Taylor series expansions as follows:

$$\begin{aligned} \Delta u_{FDI} &= u_{FDI} - u = \frac{x(t)}{\Delta t} (e^{A\Delta t} - 1 - A\Delta t) = \frac{x(t)}{\Delta t} \left[\frac{1}{2}(A\Delta t)^2 + \frac{1}{4}(A\Delta t)^3 + \frac{1}{8}(A\Delta t)^4 + \dots \right] \\ &= Ax \sum_{n=1}^{\infty} \left(\frac{A\Delta t}{2} \right)^n = u \sum_{n=1}^{\infty} \left(\frac{A\Delta t}{2} \right)^n \end{aligned} \quad (6)$$

$$\begin{aligned} \Delta u_{CDI} &= u_{CDI} - u = \frac{x(t)}{\Delta t} \left(e^{\frac{A\Delta t}{2}} - e^{-\frac{A\Delta t}{2}} - A\Delta t \right) = \frac{x(t)}{\Delta t} \left[\frac{2}{4} \left(\frac{A\Delta t}{2} \right)^3 + \frac{2}{16} \left(\frac{A\Delta t}{2} \right)^5 + \frac{2}{64} \left(\frac{A\Delta t}{2} \right)^7 + \dots \right] \\ &= Ax \sum_{n=1}^{\infty} \left(\frac{A\Delta t}{4} \right)^{2n} = u \sum_{n=1}^{\infty} \left(\frac{A\Delta t}{4} \right)^{2n} \end{aligned} \quad (7)$$

Similarly, the bias errors of the velocity component v are determined for FDI and CDI, respectively, as

$$\Delta v_{FDI} = -Ay \sum_{n=1}^{\infty} \left(\frac{-A\Delta t}{2} \right)^n = v \sum_{n=1}^{\infty} \left(\frac{-A\Delta t}{2} \right)^n \quad (8)$$

$$\Delta v_{CDI} = -Ay \sum_{n=1}^{\infty} \left(\frac{-A\Delta t}{4} \right)^{2n} = v \sum_{n=1}^{\infty} \left(\frac{-A\Delta t}{4} \right)^{2n} \quad (9)$$

Since $A\Delta t$ is usually a small, dimensionless value, e.g. in the current test case $A\Delta t < 0.07$, and the bias error of CDI is in a higher order of the small value than that of FDI, the bias error of CDI is much smaller than FDI. Ignoring the higher order terms ($n > 1$), the total bias errors of each algorithm are simply determined as follows:

$$\Delta V_{FDI} = \sqrt{(x^2 + y^2) \left(\frac{A^2 \Delta t^2}{2} \right)^2} = \frac{A^2 \Delta t}{2} r \quad (10)$$

$$\Delta V_{CDI} = \sqrt{(x^2 + y^2) \left(\frac{A^3 \Delta t^2}{16} \right)^2} = \frac{A^3 \Delta t^2}{16} r \quad (11)$$

Eq. (10) and (11) indicate that the bias errors of the four-roll mill PIV tests are proportional functions of radius r . To confirm this, five hundred of synthetic PIV recording pairs are generated according to the theoretical velocity distribution of the four-roll mill flow with 0.04 mm/s at the corner of the measurement area, where the corresponding particle image displacement is 30 pixels. The particle images are similar to that in the real PIV recordings: diameter of 3~6 pixels, brightness of 100~250, particle image number of 10240. These synthetic PIV recording pairs are, at first, evaluated with correlation-based FDI and CDI algorithms without image correction. The error distributions on the radial positions, obtained by statistically analyzing the evaluation results, are given in Fig. 7. The bias errors are determined by averaging individual error maps obtained through subtracting the known (given) displacement vectors from the evaluated vector maps. The random error is defined here as the root-mean-square (RMS) difference between the

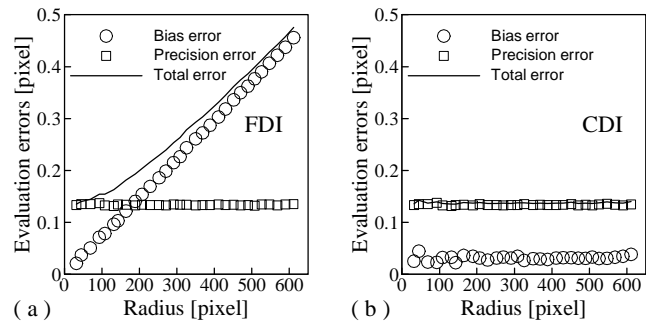


Fig.7: Dependences of evaluation errors on the radial position for using FDI (a) and CDI (b) without image correction

individual vectors and the mean at certain evaluation spot. The total error is the root-sum-square (RSS) of the bias and the random error. Fig. 7a clearly shows that the bias error of FDI is proportional to the radial position. The bias error of CDI looks independent on the radial position (Fig. 7b), because its gradient is very small and within the bias error variation that results from the limited sample number for the statistical analysis. Fig. 7 also shows that the random (precision) errors of FDI and CDI are on the same level and independent of the radial position. For FDI the total error is dominated by the bias error at radial positions greater than 200 pixels, whereas for CDI the random error dominates in the whole area.

4.2.

Effect of the image correction

The random error level shown in Fig. 7 is very high and cannot be reduced by replacing FDI with CDI. However, using the image correction technique can effectively reduce the random evaluation error. In order to demonstrate the effects of the image correction method on the evaluation errors, the 500 synthetic PIV image pairs are again evaluated with the FDI and CDI algorithm but in combination with the 4-point image correction method. The results in Fig. 8 indicate that the image correction does not noticeably change the bias error distribution but effectively reduces the random (precision) evaluation error (here by half).

4.3

Reduction of peak locking effect

The peak locking effect has always been a serious concern when evaluating digital PIV recordings, especially in the investigations of turbulent structure and vorticity distribution. Gui and Wereley (2001) discussed the mechanism of the peak-locking phenomenon in detail and suggested a continuous window shifting technique to minimize the peak-locking effect. They found that the worst peak-locking occurs when combining the correlation-based interrogation algorithm with discrete window shifting. However, the central difference image correction technique avoids the discrete window shifting, and it is equivalent to the continuous window shifting technique when there is no image distortion. As an example, the histograms of the evaluated particle image displacements using the discrete central difference interrogation (DCDI) and the central difference image correction (CDIC) method are given in Fig. 9 for the overlapped PIV recording pair in the case of cylinder rotation speed of 10 steps/second and $\Delta t=4$ s. Theoretically the histograms should be flat and smooth, because the distribution density of the velocity components in the four-roll mill is uniform. However, as shown in Fig. 9(a) the particle image displacements obtained with the DCDI method are obviously concentrated to integer pixels, so that a very strong peak-locking effect is observed. Fig. 9(a) also shows that the peaks at even pixel numbers are higher than these at odd pixel numbers. This phenomenon may result from overlapping successive PIV recordings. When using the CDIC method, the strong peak-locking effect cannot be observed (Fig. 9b).

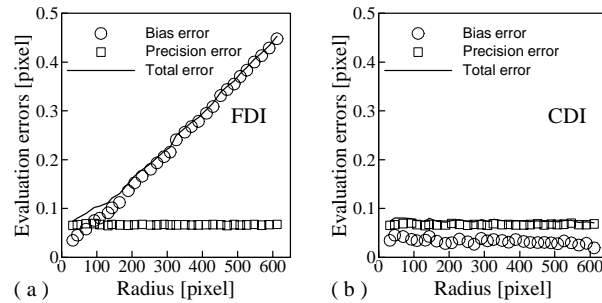


Fig.8: Dependences of evaluation errors on the radial position for using FDI (a) and CDI (b) with image correction

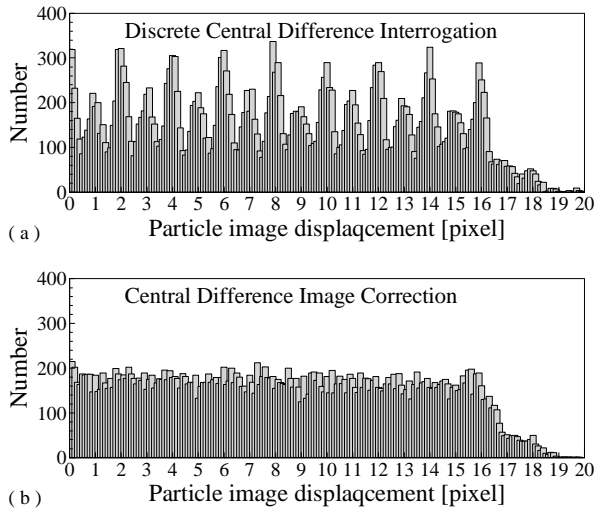


Fig.9: Histograms of the particle image displacements in a four-roll mill test case using the discrete CDI (a) and the CDIC (b) method

5

Experiment results

The direct (raw) results of the four-roll mill PIV tests are velocity vector maps. With a quantitative analysis of the vector maps the distributions of the velocity components (u , v) on the coordinates (x , y) can be experimentally determined for different test cases. Since the evaluation of the PIV recording pairs are conducted on a 30×30 uniform grid structure, in each column and each row 30 values are used to determine the mean and standard deviation of u and v , respectively. Fig. 10 provides the post-processed results for the test case of cylinder rotation speed of 400 steps/second. In the figure the error bars show the precision error, i.e. twice the standard deviation for a 95% confidence level, and the two lines are least square fits of the mean values of u and v , respectively. In this case the experimentally determined factor A has a difference of 0.0007 [1/s] (i.e. relatively 0.2%) between the two coordinate directions, which can be explained as the misalignment of the PIV camera view.

The experimentally determined factor A and its bias error bar are given in Fig. 11 for three test cases with different cylinder rotation speeds. It is shown that factor A is a linear function of the cylinder rotation speed. The error bars represent the bias errors most likely resulting from a misalignment of the PIV camera view.

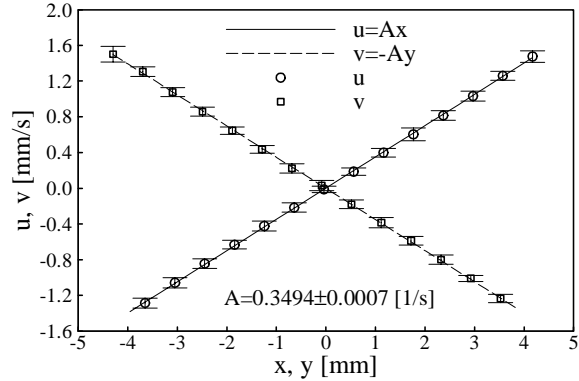


Fig.10: Distributions of mean velocity components and precision errors in the four-roll mill at cylinder speed of 400 steps/second

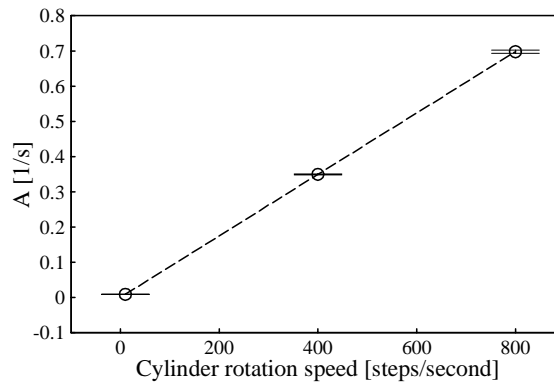


Fig.11: Dependency of factor A on the cylinder rotation speed

6

Summary and conclusions

The central difference image correction (CDIC) method described in this paper combines features of the central difference interrogation, image pattern correction and continuous window shifting. Using the new algorithm for evaluating digital PIV recordings can minimize the bias errors resulting from spatial velocity gradients, effectively reducing the random evaluation error caused by the image pattern distortion, and avoiding the strong peak-locking effect. As a multi-pass algorithm, four to five iterations are generally necessary for using the CDIC method to get an accurate, converged result, although various numerical schemes common in the literature could be used to accelerate convergence. In comparison to the adaptive discrete window shifting techniques with the same computation window, the CDIC method needs about 75% more computation time.

A 4-point image correction scheme is suggested for the CDIC method. Theoretically, a higher accuracy might be achieved when using the particle image displacements of 9 or more points in the interrogation window to correct the distorted image pattern. However, in practice the evaluation error of the 4-point scheme converges to a much lower level error than that of the 9-point scheme. Investigations in this paper also show that when combining CDIC with the correlation-based interrogation, both higher evaluation accuracy and lower computational cost can be achieved than combining CDIC with the correlation-based tracking.

The PIV experiment accurately determines the velocity field in the four-roll mill and confirms the linear distributions of the velocity components on the coordinates and the roller speed. The test results are valuable for understanding the four-roll mill flow and developing new devices.

Acknowledgements

This work was supported by the Indiana 21st Century Research and Technology Fund, and the Integrated Detection of Hazardous Materials (IDHM) Program – a Department of Defense project managed jointly by Center for Sensing Science and Technology, Purdue University, and Naval Surface Warfare Center, Crane, Indiana. Thanks to Derek Tretheway and Professor Gary Leal for making images from the four-roll mill experiments available to us.

References

- Bentley BJ; Leal LG** (1986a) An experimental investigation of drop deformation and breakup in steady, two-dimensional linear flows. *J. Fluid Mech.* 167, 241
- Bentley BJ; Leal LG** (1986b) A computer controlled four-roll mill for investigation of particle and rope dynamics in two-dimensional linear shear flows. *J. Fluid Mech.* 167, 219
- Cowen EA; Monismith SG** (1997) A hybrid digital particle tracking velocimetry technique. *Exp Fluids* 22: 199-211
- Guller GG; Leal LG** (1981) Flow birefringence of concentrated polymer solutions in two-dimensional linear flows. *J. Polym. Sci. Polym. Phys.* 19, 557
- Gui L; Merzkirch W** (1996) Phase-separation of PIV digital mask technique. *ERCOFTAC Bulletin* 30: 45-48
- Gui L; Merzkirch W** (1998) Generating arbitrarily sized interrogation windows for correlation-based analysis of particle image velocimetry recordings. *Exp. Fluids* 24: 66-69
- Gui L; Merzkirch W** (2000) A comparative study of the MQD method and several correlation-based PIV evaluation algorithms. *Exp. Fluids* 28: 36-44
- Gui L; Wereley ST** (2001) A correlation-based continuous widow shift technique for reducing the peak locking effect in digital PIV image evaluation. Submitted to *Exp. Fluids*
- Higdon JJJ** (1993) The kinematics of the four-roll mill. *Phys. Fluids A* 5 (1), January 1993, 274-276
- Huang HT; Fiedler HE; Wang JJ** (1993) Limitation and improvement of PIV; Part II: Particle image distortion, a novel technique. *Exp Fluids* 15: 263-273
- Keane RD; Adrian RJ** (1993) Theory and simulation of particle image velocimetry. In: *Laser anemometry advances applications*, 5th International Conference, Veldhoven, Netherlands, 23-27 August, Proc SPIE Series, vol 2052, pp 477-492
- Rumscheidt FD; Masno SG** (1961) Particle motions in sheared suspensions XI. Internal circulation in fluid droplets (Experimental)". *J. Colloid Sci.* 16, 210
- Taylor GI** (1934) The formation of emulsions in definable fields of flow. *Proc. R. Soc. London Ser. A* 146, 501
- Tokumaru PT; Dimotakis PT** (1995) Image correlation velocimetry. *Exp Fluids* 19: 1-15
- Torza S** (1975) Shear-induced crystallization of polymers; I: The four-roller apparatus. *J. Polym.Sci. Polym. Phys.* 13, 43
- Wereley ST, Santiago JG, Meinhart CD, Adrian RJ** 1998, *Velocimetry for MEMS Applications. Proc. of ASME/DSC*, Vol. 66, (*Micro-fluidics Symposium*, Nov. 1998, Anaheim, CA)
- Wereley ST, Meinhart CD** 2000, Accuracy improvements in particle image velocimetry, 10th *International Symposium on "Applications of Laser Techniques to fluid Mechanics"*, Lisbon, Portugal, July
- Wereley ST, Meinhart CD** 2001, Second-order accurate particle image velocimetry, *Exp. Fluids* (in press)
- Wereley ST; Gui L; Meinhart CD** (2001), Flow measurement techniques for the microfrontier. 30th Aerospace Science Meeting & Exhibit, January 8-11, Reno, Nevada, (also) accepted by *AIAA Journal*
- Westerweel J; Dabiri D; Gharib M** (1997), The effect of a discrete window offset on the accuracy of cross-correlation analysis of digital PIV recordings, *Exp. Fluids* 23, 20-28
- Willert CE** (1996), The fully digital evaluation of photographic PIV recordings. *Appl. Sci. Res.* 56, 79-102